AGU PUBLICATIONS

Geochemistry, Geophysics, Geosystems

RESEARCH ARTICLE
10.1002/2013GC005141

Seafloor basalt alteration and chemical change in the ultra thinly sedimented South Pacific

Guo-Liang Zhang[1] and Christopher Smith-Duque[2]

[1]Key Laboratory of Marine Geology and Environment, Institute of Oceanology, Chinese Academy of Sciences, Qingdao, China, [2]National Oceanography Centre, University of Southampton, Southampton, UK

Key Points:
- Ocean crust alteration in the South Pacific continues even in ~100 Ma crust
- Low sedimentary rates (m/Myr) facilitates continued fluid flow in ocean crust
- Alteration style and intensity are closely tied to crustal structure

Supporting Information:
- Readme
- Supplementary 1. Methods
- Supplementary Figure S1
- Supplementary Tables T1–T4

Correspondence to:
G.-L. Zhang,
zhangguoliang@qdio.ac.cn

Citation:
Zhang, G.-L., and C. Smith-Duque (2014), Seafloor basalt alteration and chemical change in the ultra thinly sedimented South Pacific, *Geochem. Geophys. Geosyst.*, *15*, 3066–3080, doi:10.1002/2013GC005141.

Received 14 NOV 2013
Accepted 11 JUL 2014
Accepted article online 15 JUL 2014
Published online 31 JUL 2014

Abstract Determining the relationship between ocean floor basalt alteration and sedimentation is fundamental to understanding how oceanic crust evolves with time. Ocean floor basalts recovered at IODP Sites U1365 (~100 Ma) and U1368 (~13.5 Ma) in the South Pacific have been subjected to remarkably low sedimentation rates (0.71 and 1.1 m/Myr^{-1}, respectively). We report detailed petrographic and geochemical analysis of basalt cores from these sites in order to investigate what impact sediment insulation has on seafloor alteration beyond 10–15 Myr of ocean crust formation. Both sites exhibit low-temperature (<150°C) alteration (e.g., iron-hydroxides, carbonate, and quartz) within a predominantly oxidative regime, albeit with markedly different alteration styles and intensity. Alteration at Site U1365, which is predominantly composed of sheet flows, occurs mainly near sheet flow boundaries and fractures. In contrast, Site U1368 comprises interlayered pillows and thin sheet flows that have been subjected to relatively even levels of alteration. Variation of alteration style and intensity between Sites U1365 and U1368 appear closely tied to lithology and crustal structure. Although alteration-induced elemental changes at both sites are similar in, e.g., increasing K, Rb, U, Ba, and Fe^{3+} and decreasing Fe^{2+}, Ca, and Ni, they show distinct differences in Th, which is significantly decreased at Site U1365 but relatively constant at Site U1368. At both sites enrichment of LREEs relative to HREEs is ascribed to alteration. The greater vein abundance and notably higher Fe^{3+}/TiO_2, K_2O/TiO_2, LOI/TiO_2, and Rb/TiO_2 ratios of representative samples at Site U1365 compared to Site U1368 are attributed to increased alteration intensity. This is mirrored by greater overall chemical change (Fe_2O_3, FeO, CaO, K_2O, Li, Rb, Pb, and U) observed at Site U1365 than those of Site U1368 and other DSDP/ODP sites between 6 and 46 Ma. Since both Sites U1365 and U1368 endured only minimal sedimentation, we attribute the differences in overall chemical change across the two sites to duration of exposure to seawater.

1. Introduction

Seawater circulation and subsequent alteration of ocean crust play important roles in chemical exchange between the hydrosphere and lithosphere [e.g., *Staudigel and Hart*, 1983; *Alt and Teagle*, 2003; *Paul et al*., 2006] and has a profound influence on arc volcanics and mantle composition through subduction [e.g., *Hauff et al*., 2003]. A wealth of research has been dedicated to constraining when ocean floor basalt alteration ceases and what factors are involved.

Petrographic relationships and radiometric dating of secondary mineral assemblages at young sites suggest that most basement alteration takes place within 10–15 Myr after crustal formation [e.g., *Staudigel et al*., 1981a; *Richardson et al*., 1980; *Thompson*, 1983; *Staudigel et al*., 1986]. In addition, comparisons between old (e.g., 162Ma ODP Site 801) and young (e.g., 6Ma ODP Site 504B) ocean crust suggest that most alteration is complete within several million years of crust formation [e.g., *Alt et al*., 1992; *Alt and Teagle*, 2003; *Talbi and Honnorez*, 2003; *Hauff et al*., 2003]. Furthermore, observed peaks in seismic velocity in ~8–10 Ma crust [*Grevemeyer et al*., 1999] and maturity in *P* wave velocity in 10 Ma upper oceanic crust [e.g., *Nedimović et al*., 2008] are both interpreted to represent the cessation of major hydrothermal circulation in ocean crust by precipitation of secondary minerals filling nearly all voids. Similarly, observations of heat flow models imply that precipitation of secondary minerals effectively seal the crust, leading to reduced fluid flow and, therefore, reduced hydrothermal cooling [e.g., *Gillis and Robinson*, 1988; *Grevemeyer et al*., 1999; *Jarrard et al*., 2003]. This process is thought to be enhanced by sediment blanketing [*Rohr*, 1994; *Nedimović et al*., 2008]. Indeed, many researchers ascribe early cessation of ridge flank hydrothermal activity to rapid sedimentary burial [e.g., *Lister*, 1972; *Anderson and Hobart*, 1976; *Jacobson*, 1992; *Alt and Teagle*, 2003].

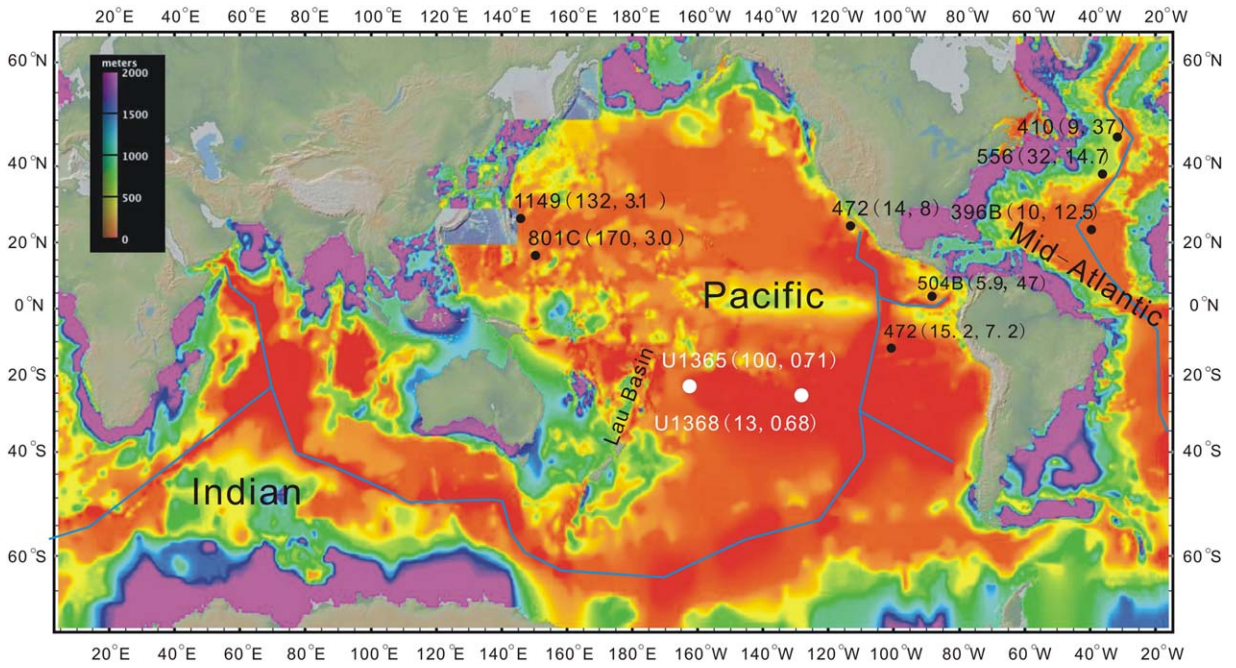

Figure 1. Location of IODP Site U1365 and Site U1368 and global distribution of sediment thicknesses. The numbers in the parentheses besides the site name indicate the basement age and sedimentary rate (m/Myr). Data for the sediment thickness distribution are from *Divins* [2003].

Despite considerable evidence to suggest that the majority of alteration is complete within ~15 Ma, age dating of secondary minerals and mineralogical studies in some DSDP/ODP sites indicate continued fluid flow in oceanic crust much older than 10–15 Ma [e.g., *Hart and Staudigel*, 1986; *Burns et al*., 1992; *Talbi and Honnorez*, 2003]. *Stein and Stein* [1994] attribute the discrepancy between the global modeled and measured heat flows in ~50 Ma global ocean crust to hydrothermal fluid flow. More recent estimates suggest that hydrothermal circulation takes place in oceanic crust in excess of 60–65 Ma [*Johnson and Pruis*, 2003; *Hasterok et al*., 2011]. Furthermore, *Jarrard et al*. [2003] suggest on the basis of studies on changes in matrix density of ODP basement cores that crustal alteration continues, although at a decreasing rate, throughout the life of the ocean crust.

Since all previous DSDP/ODP/IODP basement cores of ocean crust were located in areas with sedimentary rates >4 m/Ma [*Johnson and Pruis*, 2003], it has been difficult to estimate how sediment blanketing affects alteration in ocean crust through time. Furthermore, questions remain regarding the roles of lithology, crustal structure, and local heterogeneities (e.g., topography) in controlling the style, duration, and intensity of low-temperature alteration in upper oceanic crust. How sediment is distributed on the ocean floor is thought to influence fluid circulation in underlying ocean crust [e.g., *Snelgrove and Forster*, 1996; *Giambalvo et al*., 2000]. Selective extraction and fluid flow may be facilitated by conduits at topographic highs, e.g., seamounts [e.g., *Wheat and Mottl*, 2000; *Fisher et al*., 2003a, 2003b; *Hutnak et al*., 2008]. IODP Sites U1365 (100 Ma) and U1368 (13.5 Ma) offer a unique opportunity to study how lithology and structure affect low-temperature alteration of upper oceanic crust. Both sites are located within the South Pacific Gyre (Figure 1) [*D'Hondt et al*., 2011], a region where low productivity over tens of millions of years has led to ultralow-average sedimentary burial rates of between 0.1 and 1 m/Ma, among the world's lowest [*D'Hondt et al*., 2009]. In this study, we use visual core description and major and trace element data of basalts from the South Pacific Gyre to investigate the structural controls on alteration and its timing. Our comparison of alteration at Sites U1365 and U1368 with those of other drill sites provides new insight on the relative role of sediment blanketing and ocean crust structure in controlling the style, intensity, and duration of alteration in upper ocean crust. Characteristics of crustal alteration at Site U1365 are also important for understanding the composition of upper oceanic crust subducting into the southwest Pacific subduction zone.

2. Geological Setting and Sampling

Site U1365 is located in the western margin of the South Pacific Gyre, ~800 km to the east of the Tonga-Kermadec trench (Figure 1). The crust at Site U1365 was accreted during the Cretaceous Superchron (84–120 Ma) from the Osbourn trough with a medium to fast spreading rate [*Zhang et al*., 2012]. However, the

basement age and spreading rate at Site U1365 are poorly constrained. Site U1365 is located in an area with relatively smooth topography with an abyssal hill spacing of 5–8 km. Three nearby seamounts with a maximum relief of 400 m border the area. Basement at Site U1365 is covered by ~71 m thick sediment, and assuming a formation age of 84–120 Ma, we derive an average sedimentation rate of 0.71 (±0.12) m/Myr. A lack of biostratigraphic data precludes a more detailed description of the sedimentary burial history at Site U1365.

Site U1368 is located in the center of the South Pacific Gyre, ~3000 km to the west of the EPR at 25°S (Figure 1). The crust at Site U1368 was accreted from the EPR during Magnetic Chron 5ABn, indicating a crustal age range of 13.4–13.6 Ma. According to the NUVEL-1 model [*Argus and Gordon*, 1991], Site U1368 has a full spreading rate of 160 mm/yr. Basement at Site U1368 is overlain by 15 m of sediment with an average accumulation rate of 1.1 m/Myr. Like Site U1365, it is located in an area of smooth topography and bordered by several seamounts (~500 m high).

Following 53.2 m of drilling into basement at Site U1365, 39.66 m of sheet flows were recovered (74.6% recovery), and no sediment/basement interface was recovered [*D'Hondt et al*., 2011]. At Site U1368, 31.74 m of flows and pillow lavas was recovered from 103.3 m of basement drilling (30.7% recovery). The sediment/basement interface was recovered in Core U1368-2R [*D'Hondt et al*., 2011].

3. Methods

3.1. Petrographic Description

Primary igneous texture, composition, and alteration of recovered basalt, including classification of lithologic units (Figure 2), alteration color, vesicle filling, and vein distribution (vein shape, thickness, and mineral fillings) were described in detail. Secondary mineral assemblages were determined by thin section observation, macroscopic observation, and XRD analyses. In this study, at least one thin section was made for each sample from Sites U1365 and U1368. Textures, secondary mineral proportions, and other alteration characteristics (e.g., color, vesicles, and veins) for each sample were determined using a petrographic microscope.

3.2. Bulk Rock Major and Trace Elements

For a comprehensive analysis of all alteration types, we selected 58 basalt samples from Site U1365 and 62 samples from Site U1368 (see Figure 2 for location within recovered basement), including samples from *Zhang et al*. [2012, 2013]. Prior to powdering and dissolution of samples for bulk rock analyses, samples were carefully selected to avoid veins. Where necessary, veins were removed by grinding.

Major elements and Cr, Sr, and V were analyzed on fused glass discs with an Axios sequential X-Ray Fluorescence Spectrometer at the Institute of Geology and Geophysics, Chinese Academy of Sciences (IGGCAS). Trace elements were analyzed by ICP-MS (Agilent 7500) using In, Rh, and Re as internal standards at Peking University. Detailed procedures and accuracy of the analytical results are shown in supporting information.

4. Results

4.1. Petrography and Secondary Minerals

4.1.1. Site U1365

Site U1365 basement comprises 17 lithologic units made up of 0.5–8 m thick sheet/massive flows. Secondary mineral phases observed include celadonite, Fe-oxyhydroxides, saponite, calcium carbonate, quartz, and sulfides. They are typically concentrated within halos that flank veins and fractures, especially near unit boundaries. Away from unit boundaries, replacement of primary mineralogy, veins, halos, and brecciation is less common. The style and intensity of alteration at Site U1365 is similar to uppermost crust from other sites [e.g., *Staudigel et al*., 1981a, 1981b; *Alt and Honnorez*, 1984; *Alt et al*., 1996; *Laverne et al*., 1996; *Paul et al*., 2006].

Based on surface area measurement on the intersecting surface of the split cores alteration halos occupy ~12% of the recovered core. By cross-referencing our macroscopic observations of color with secondary mineral identification within halos by thin section observation, we estimate the abundances of each halo type (color) and their dominant secondary mineralogy as follows: dark green to dark gray (celadonite): 1.9%, green to brown/orange (saponite): 5.1%, red to brown (Fe-oxyhydroxides): 3.5%, and complex (multiple mineral phases): 2%. Alteration extent is typically greatest within green to brown and red-brown halos which exhibit 8%–20% replacement whereas alteration in dark green to dark gray halos is slight (~2%–5%).

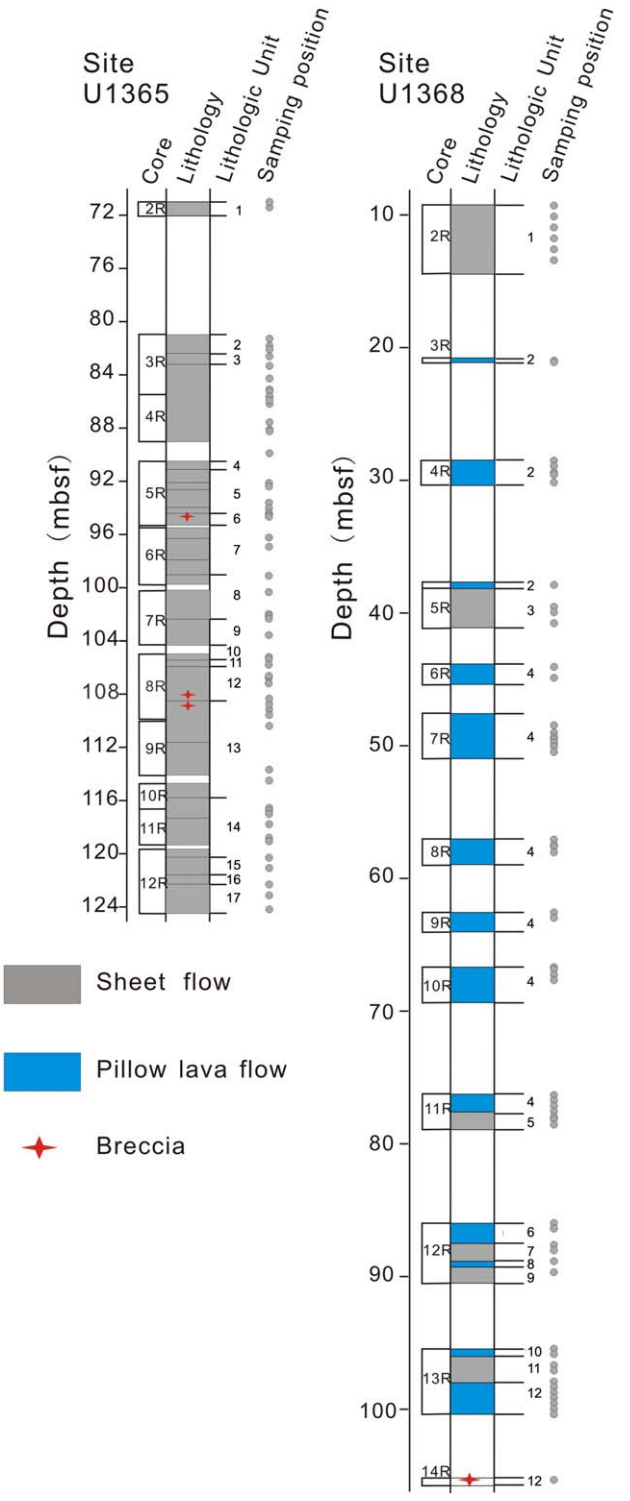

Figure 2. Stratigraphy (flow type) of recovered cores from Site U1365 and U1368 and sampling positions.

Breccias at Site U1365 are rare. Interval U1365E-5R-4, 57–63 cm, at ~23 m subbasement (msb) depth, is composed of a mixed breccia containing basaltic and glassy clasts in a matrix of carbonate and numerous altered glass fragments. Two additional breccia fragments at interval U1365E-8R-3, 130–134 cm (~36 msb), were recovered. These include a basaltic breccia with a cement of calcium carbonate, and a hyaloclastite composed of altered glass in a matrix of carbonate, quartz, and altered glass. Three pieces of a dark rock, composed almost entirely of calcium carbonate and ~3% opaque, were recovered at intervals U1365E-5R-1 (0–4) and U1365E-6R-1 (14–26). These pieces are thought to represent extreme interflow alteration, with near total replacement of the original groundmass. The total volume of secondary minerals in veins and breccia (calculated from surface area of core and normalized to account for recovery) accounts for 0.8% and 0.2% of the core, respectively. Vesicles make up <1% of the core, but can vary between <0.1% and 15% in individual units. They are partially to totally filled with celadonite, Fe-oxyhydroxides, saponite, and calcium carbonate.

Crosscutting relationships, vesicle and fracture filling order, and halo overprinting relationships indicate an oxidative "open" phase of fluid flow dominated by iron-oxyhydroxides and celadonite which was followed up by more restrictive fluid flow resulting in saponite and minor sulfide precipitation. Carbonate and zeolites in veins that crosscut all other phases appear to represent multiple episodes of late stage fluid flow.

4.1.2. Site U1368

Site U1368 basalts comprises 13 lithologic units that alternate between pillow lavas (six units) and sheet flows (six units) with one breccia unit at the bottom. Secondary mineral phases include (in order of

abundance) saponite, Fe-oxyhydroxides, calcium carbonate, celadonite, zeolite, quartz, and rare sulfides, which is similar, albeit in lower abundances, to Site U1365. The majority of alteration at Site U1368 consists of groundmass replacement (~1–10% by volume) within discrete patches and vein-flanking halos.

We apply the same method used for Site U1365 to estimate halo type and abundances in Site U1368. Halos comprise ~8.4% of Site U1368 basalt core, including (with % of recovered core): (1) Green-brown, saponite-dominant (6%); (2) complex, composed of two or more overlapping secondary mineral assemblages (1.2%); (3) dark green, with celadonite (1%); and (4) red-brown, Fe-oxyhydroxide-rich (0.2%). Alteration extent within halos is typically slight (~2–10% replacement) though less common red-brown halos exhibit 5–15% replacement. Halos are most abundant in Cores U1368F-2R, 3R, and 12R to 14R.

Vesicles occur in all igneous units and range from <0.1% to 10% (average ~0.5%) in abundance. Vesicles are typically empty to partially filled with secondary minerals, including celadonite, Fe-oxyhydroxides, saponite, zeolites, silicates, and calcium carbonate. Zeolite-filled vesicles occur within Cores U1368F-2R and 3R only. Breccia recovered at interval U1368F-14R-1, 43–150 cm (~97 msb) comprises clasts composed of angular glass fragments with rims that are variably altered to saponite rims (90% of clasts) and basalt fragments (10% of clasts) with quartz cement. It is defined as a volcaniclastic hyaloclastite and interpreted to represent a collapse breccia [*D'Hondt et al*., 2011]. Overall ~1% of the recovered core comprises veins and breccia.

At Site U1368, celadonite is observed as the earliest phase. Fe-oxyhydroxides appear to have co-precipitated with celadonite, but also overprinted celadonite. Saponite overprints celadonite and Fe-oxyhydroxides, which in turn is overprinted/crosscut by late stage calcium carbonate veins, silicates, and zeolites. For secondary sulfides, no crosscutting relationships or overprinting was observed; however, the overall order of secondary mineral emplacement is similar to the filling order observed within vesicles at Site U1365. At Site U1368, alteration intensity at both pillow lavas and sheet flows is observed to decrease away from chilled margins and flow boundaries; however, the extreme contrasts between alteration at fluid/rock interaction zones observed at Site U1365 are largely absent from Site U1368.

4.2. Veins

Site U1365 basement contains on average 14.1 veins/metre. They are typically subhorizontal, and range from 0.1 to 15 mm thick. In order of abundance veins are composed of carbonate (1%), celadonite (0.5%), saponite (0.18%), Fe-oxyhydroxides (0.18%), quartz (0.04%), and pyrite (0.01%), and they collectively make up 2% of the recovered core. The order of vein filling, as determined by crosscutting relationships is as follows: celadonite, Fe-oxyhydroxides, saponite, and finally calcium carbonate, which is typical for upper basement sites [e.g., *Staudigel et al*., 1981a, 1981b; *Alt and Honnorez*, 1984; *Alt et al*., 1996; *Laverne et al*., 1996; *Paul et al*., 2006]. Zeolite and quartz are associated with calcium carbonate only, which implies formation during or after calcium carbonate precipitation. Many veins exhibit multiple episodes of calcium carbonate infill.

At Site U1368, we report an average vein abundance of nine veins/meter and range from <0.1–4 mm in thickness. Secondary minerals that form veins at Site U1368 include, in order of abundance, saponite (0.34%), Fe-oxyhydroxides (0.13%), quartz (0.12%), celadonite (0.08%), calcium carbonate (<0.01%), and minor phases (unidentified clays, chalcedony, zeolite, and secondary sulfides). Veins collectively make up 0.6% of the recovered core. Though secondary mineral phases within veins are similar to Site U1365, overall volumes are much lower at Site U1368. Unlike Site U1365, carbonate and celadonite are relatively minor phases at Site U1368. The order of vein filling as observed by crosscutting relationships suggests early and contemporaneous formation of celadonite and iron-oxyhydroxides, followed by saponite and late stage calcium carbonate. Vein filling minerals at Site U1368 are indicative of a low-temperature environment [e.g., *Hart*, 1970; *Böhlke et al*., 1980; *Alt et al*., 1992; *Pichler et al*., 1999].

Data for veins (vein abundance, vein, and halos thicknesses) were normalized to the amount of material recovered (supporting information Table S1) and are shown in Figure 3. Site U1365 veins are generally thicker and contain a significantly higher abundance of carbonate, saponite, celadonite, and pyrite veins than Site U1368.

4.3. Bulk Rock Chemistry

Major and trace element data for representative samples of Sites U1365 and U1368 are shown in Table 1 (for all data, see supporting information Table S2). Downhole elemental variations of Site U1365 and U1368

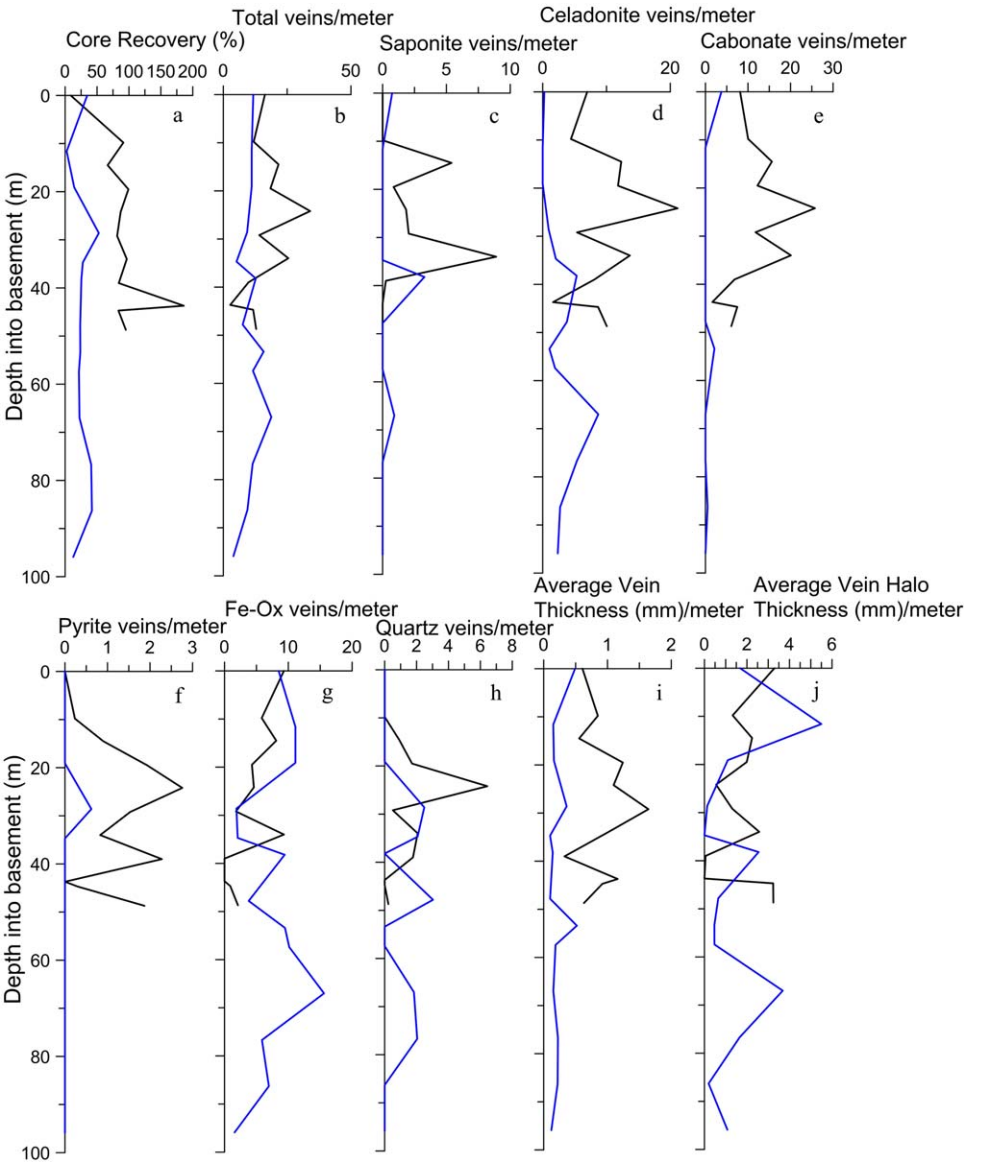

Figure 3. Downhole variations of (a) core recovery (%), distributions (veins per meter) of (b) total veins, (c) saponite veins, (d) celadonite veins, (e) carbonate veins, (f) pyrite veins, (g) Fe-oxidize, (h) quartz veins, (i) average vein thicknesses (mm/m), and (j) average vein halo thicknesses (mm/m). Black line, U1365; blue line, U1368.

basalts are shown in Figure S1. Comparing the least altered samples from each site, we find that Site U1365 MgO concentrations are high, while Fe_2O_3 and SiO_2 are low compared to Site U1368, indicating lower differentiation degrees for Site U1365 lavas. Downhole variations for fluid-immobile elements, such as Ti, P, Zr, La, Lu, and Hf, are similar across both sites, though overall concentrations for Site U1365 are lower than those for Site U1368 (Figure S1). Measured concentrations of fluid mobile elements, such as K, Ca, and Ba [e.g., *Alt et al*., 1992; *Pichler et al*., 1999; *Talbi and Honnorez*, 2003; *Schramm et al*., 2005], exhibit a greater range in concentration at Site U1365 than Site U1368. For both sites, U/Pb ratios of many samples reach the requirement for a HIMU mantle end-member [e.g., *Sun and McDonough*, 1989].

5. Discussion

5.1. Alteration-Induced Element Transport

Secondary mineral percentages from petrographic observation (supporting information Table S3) versus bulk rock major and trace elements and LOI (Figure 4) are used to assess the link between elemental

Table 1. Compositions of Major (wt %) and Trace (μg/g) Elements for Representative Samples From Sites U1365 and U1368

Hole	U1365E	U1365E	U1365E	U1365E	U1365E	U1365E	U1365E	U1365E	U1368F	U1368F	U1368F	U1368F	U1368F	U1368F	U1368F	U1368F
Core	3R	3R	4R	4R	5R	6R	7R	7R	2R	5R	6R	7R	8R	11R	13R	13R
Section	3-W	4-W	1-W	1-W	4-W	4-W	1-W	3-W	1-W	3-W	1-W	2-W	1-W	1-W	1-W	3-W
Interval	33–37	68–70	22–24	24–25	53–57	8–10	41–45	2–4	13–17	9–14	119–123	8–13	31–36	133–137	114–115	131–135
SiO_2	46.35	48.24	50.15	49.18	47.34	45.29	47.65	45.49	47.98	49.68	49.24	51.20	50.73	47.64	49.48	48.21
TiO_2	1.10	1.20	1.44	1.40	1.48	1.00	0.87	0.97	1.91	2.38	2.27	2.43	2.35	2.35	2.31	2.25
Al_2O_3	17.19	17.18	16.42	16.07	15.22	14.99	18.44	17.01	16.48	13.06	13.78	15.15	14.34	13.48	13.79	14.28
TFe_2O_3	8.84	9.32	7.57	9.99	11.52	11.21	8.36	8.98	9.32	15.11	13.19	8.29	10.96	16.05	12.91	13.42
MnO	0.13	0.15	0.13	0.13	0.18	0.13	0.13	0.04	0.12	0.20	0.19	0.18	0.19	0.20	0.18	0.20
MgO	10.78	7.09	6.66	6.25	6.44	6.99	8.50	4.32	6.72	5.95	5.84	6.30	6.05	4.99	6.75	5.77
CaO	10.20	12.06	12.22	11.59	10.22	13.15	12.48	6.02	10.67	10.15	10.97	11.93	11.27	10.39	10.79	10.97
Na_2O	2.20	2.57	2.96	2.90	2.42	2.13	2.14	0.99	3.19	2.97	2.71	3.02	2.90	2.64	2.79	2.73
K_2O	0.08	0.23	0.39	0.49	1.78	0.88	0.05	7.03	0.69	0.12	0.56	0.18	0.28	0.65	0.15	0.50
P_2O_5	0.09	0.10	0.13	0.12	0.11	0.07	0.07	0.06	0.33	0.23	0.24	0.26	0.26	0.26	0.24	0.24
LOI	3.24	1.74	1.92	1.66	2.92	3.98	1.00	9.45	1.78	0.04	0.90	0.68	0.58	1.14	0.34	1.06
Total	100.20	99.89	99.98	99.79	99.63	99.82	99.68	100.36	99.20	99.89	99.89	99.62	99.90	99.80	99.73	99.64
FeO	5.31	3.18	3.22	3.02	3.63	3.45	5.32	0.60	3.55	9.47	5.34	5.19	5.70	5.12	7.77	5.48
Fe_2O_3	2.94	5.78	3.99	6.63	7.49	7.38	2.45	8.31	5.37	4.58	7.25	2.52	4.62	10.37	4.28	7.33
Li	35.2	28.4	32.1	26.3	25.1	25.7	5.9	37.1	27.1	6.4	6.9	7.4	6.2	6.9	9.4	20.8
Be	0.27	0.28	0.31	0.35	0.44	0.19	0.17	1.25	0.77	0.53	0.57	0.55	0.57	0.64	0.56	0.51
Sc	37.3	38.6	45.4	46.1	44.6	39.7	33.3	30.1	35.5	47.5	45.7	50.4	46.7	43.5	44.8	42.9
V[a]	214	232	257	273	310	268	191	174	260	445	399	432	404	401	405	380
Cr[a]	299	284	290	281	188	368	300	339	205	41	213	227	221	209	227	221
Co	38.5	38.8	40.1	35.7	33.3	34.3	41.0	10.6	40.6	44.3	38.5	81.7	55.3	33.3	44.3	40.3
Ni	72.5	69.7	46.6	50.4	44.2	57.3	97.3	122.1	111.8	35.4	47.3	133.9	90.4	47.8	83.1	63.9
Cu	49.1	57.2	62.5	49.9	41.9	33.6	69.0	199.9	48.3	54.6	44.7	66.7	52.0	44.7	46.5	49.9
Zn	52.5	62.5	73.7	66.8	83.4	62.5	57.8	115.5	70.5	115.2	107.4	118.0	117.4	93.4	112.5	103.6
Ga	14.7	15.7	16.0	16.1	16.7	14.5	14.5	9.1	17.3	19.2	18.4	20.1	19.0	17.9	18.1	18.5
Ge	5.16	5.25	4.36	5.66	6.48	5.91	4.61	5.05	4.98	7.76	7.06	4.67	5.74	8.09	6.64	7.56
Rb	1.56	5.09	3.03	7.08	22.51	13.69	0.83	42.50	8.83	0.75	13.53	1.70	4.48	18.24	1.39	10.96
Sr[a]	121	149	146	144	127	100	115	129	300	119	143	187	147	124	116	125
Y	20.1	21.8	24.4	24.2	23.2	19.0	17.3	10.9	26.5	45.9	46.1	50.6	51.0	41.8	46.1	43.2
Zr[a]	60	62	75	72	80	45	40	45	141	130	142	149	149	147	140	138
Nb	1.33	1.47	1.84	1.79	1.91	0.95	0.74	0.84	18.68	4.66	4.32	4.43	4.41	4.14	4.20	4.01
Cd	0.14	0.12	0.14	0.13	0.15	0.13	0.15	0.10	0.23	0.33	0.37	0.51	0.38	0.25	0.28	0.23
Sn	0.53	0.65	0.77	0.73	0.84	0.57	0.44	0.44	1.32	1.95	1.55	1.68	1.55	1.56	1.68	1.44
Cs	0.05	0.23	0.06	0.20	0.95	0.40	0.03	0.65	0.34	0.01	0.73	0.02	0.14	1.05	0.03	0.72
Ba	7.72	36.01	8.36	15.40	122.13	18.75	3.16	236.99	117.08	12.90	25.44	63.99	27.30	14.42	11.75	9.68
La	2.26	2.54	2.84	3.03	2.89	1.65	1.45	2.63	13.48	6.05	6.16	6.60	7.08	5.50	5.99	5.73
Ce	7.2	8.2	9.9	9.7	9.7	5.3	5.0	3.7	30.6	17.5	19.1	20.3	21.2	17.3	17.9	17.8
Pr	1.26	1.43	1.69	1.64	1.63	0.99	0.91	0.88	4.04	3.02	3.15	3.41	3.46	2.90	3.07	2.95
Nd	7.7	8.7	10.3	10.1	10.0	6.3	5.8	5.0	20.3	18.1	19.0	20.2	20.6	17.4	18.2	17.6
Sm	2.48	2.73	3.20	3.19	3.16	2.13	1.95	1.58	4.67	5.35	5.61	6.07	5.99	5.25	5.40	5.26
Eu	0.96	1.08	1.23	1.19	1.22	0.87	0.80	0.65	1.65	1.90	1.85	2.04	1.98	1.74	1.85	1.77
Gd	3.13	3.47	4.16	3.93	3.91	2.84	2.66	1.92	5.48	7.09	7.21	7.72	7.68	6.55	7.03	6.61
Tb	0.58	0.64	0.76	0.73	0.73	0.54	0.50	0.38	0.87	1.32	1.33	1.43	1.43	1.24	1.29	1.21
Dy	3.87	4.27	4.91	4.77	4.86	3.70	3.33	2.57	5.45	8.69	9.06	9.67	9.59	8.11	8.61	8.22
Ho	0.82	0.90	1.03	1.00	1.01	0.79	0.71	0.53	1.10	1.88	1.90	2.04	2.07	1.76	1.81	1.77
Er	2.40	2.68	2.96	2.92	2.99	2.30	2.09	1.59	3.15	5.60	5.55	6.02	6.11	5.14	5.33	5.14
Tm	0.37	0.42	0.46	0.46	0.48	0.36	0.33	0.27	0.49	0.90	0.91	0.96	1.01	0.84	0.88	0.84
Yb	2.46	2.72	2.97	3.00	3.06	2.36	2.13	1.87	3.03	5.80	5.84	6.32	6.54	5.50	5.65	5.41
Lu	0.38	0.41	0.44	0.44	0.46	0.36	0.32	0.27	0.44	0.87	0.87	0.91	0.97	0.79	0.85	0.79
Hf	1.97	2.21	2.60	2.56	2.75	1.72	1.47	1.56	3.92	4.50	4.73	5.07	4.97	4.78	4.64	4.50
Pb	0.43	0.45	0.33	0.44	0.65	0.45	0.68	1.23	0.86	0.86	0.72	1.11	0.67	0.62	0.76	0.58
Th	0.03	0.04	0.10	0.09	0.06	0.01	0.03	0.00	1.20	0.27	0.23	0.25	0.24	0.23	0.22	0.22
U	0.02	0.03	0.23	0.25	0.15	0.11	0.02	0.42	0.44	0.13	0.12	0.06	0.11	0.13	0.10	0.19

[a]Determined by XRF.

change and alteration. At Sites U1365 and U1368, K_2O and Rb are elevated with increasing alteration (total secondary mineral percentage). This relationship is typical of low-temperature (<150°C) alteration of upper oceanic crust [e.g., *Hart and Staudigel*, 1982; *Bach et al*., 2001; *Schramm et al*., 2005] due to the formation of K-bearing clay minerals, e.g., celadonite and saponite [*Alt et al*., 1992; *Pichler et al*., 1999; *Talbi and Honnorez*, 2003]. Basalts at Site U1365 show a general trend of increasing Ba and U with increased alteration. However at Site U1368, this trend is not clear which may be explained by the comparatively higher abundances of K_2O, Ba, Rb, and U in the least altered samples at Site U1368 compared to least altered Site U1365 samples

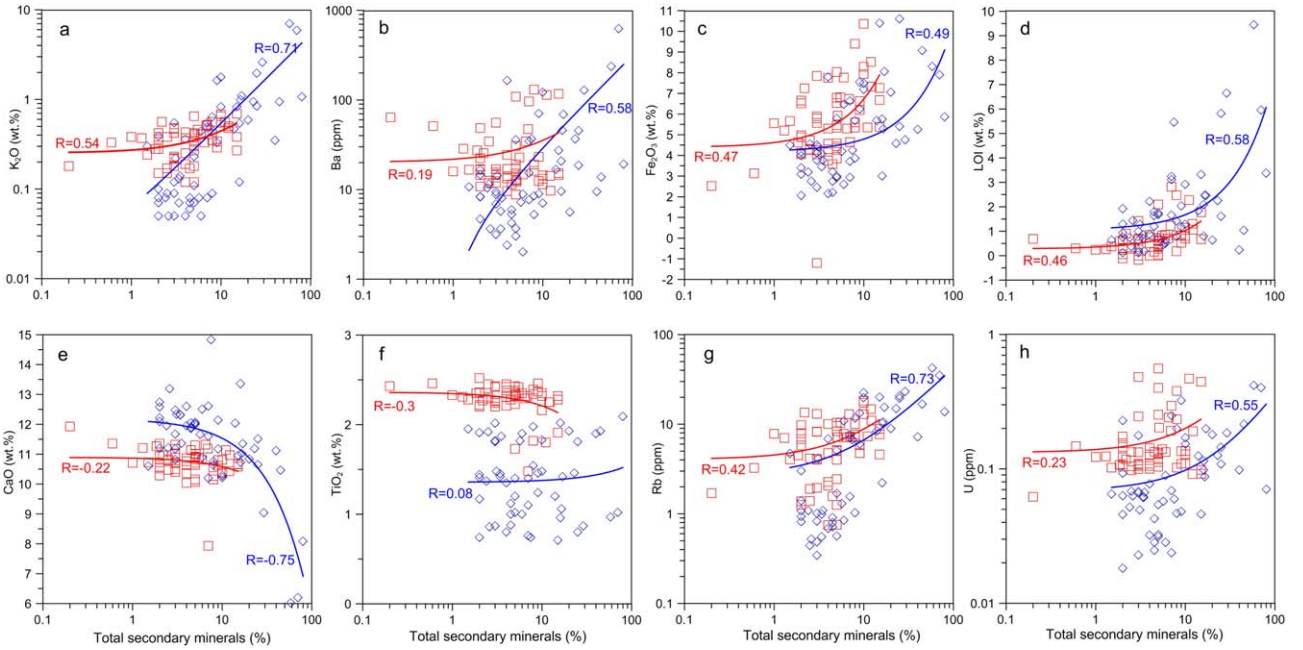

Figure 4. Relationships of total secondary minerals (%) versus (a) K_2O, (b) Ba, (c) Fe_2O_3, (d) LOI, (e) CaO, (f) TiO_2, (g) Rb, and (h) U for Sites U1365 and U1368 samples. Diamond, samples for Site U1365; square, samples for Site U1368. The blue and red lines indicate regression fit of Sites U1365 and U1368, respectively, while the R near the line shows the regression coefficient.

(Figure 4). At Site U1365, the wide range and positive trends of K_2O, Ba, Rb, and U versus total secondary mineral percentage are consistent with intensive and focused alteration. Relatively impermeable lava flows at U1365 appear to have inhibited fluid flow and subsequent alteration of flow interiors. Lower concentrations of K_2O, Ba, Rb and U and weaker trends between these elements and secondary mineral percentages, and minimal variation in concentration with depth at Site U1368 point to less intense, albeit more pervasive alteration. This may relate to the high proportion of permeable pillow lavas at U1368 facilitating open, cold seawater circulation.

The positive trend between Ba and alteration (Figure 4b) at Site U1365 is likely the result of Ba incorporation into secondary calcium carbonate from seawater. This contrasts with no clear trend between observed Ba versus secondary mineral percentage at Site U1368 (Figure 4b), where calcium carbonate is very rare (Table S3). Differences in % ferric iron (Fe_2O_3) in least altered U1368 basalts may relate to incompatibility in the magmatic processes before the initiation of magnetite crystallization; however, Figure 4c demonstrates a strong link between Fe_2O_3 and alteration at both Sites U1365 and U1368, which indicates an oxidative alteration regime. This is supported by elevated K_2O, U, and LOI, which are likely the result of clay mineral precipitation, into which K, U, and H_2O are incorporated [e.g., *Bach et al*., 2001; *Kurnosov et al*., 2008]. Decomposition of primary mineralogy (e.g., plagioclase) offers an explanation for the decrease in CaO with alteration observed in Figure 4e. Given that our samples avoided veins, the rarity of carbonate within groundmass, and the presence of veins, it seems likely that Ca was redistributed into calcium carbonate within veins.

To quantify elemental changes associated with alteration, we selected 15 and 14 altered and fresh sample pairs from Sites U1365 and U1368, respectively (Table S2). Sample pairs were subsampled from either an individual piece or from within the same lithologic unit. Pairs include dark gray to gray background ("fresh"), red-brown, greenish brown, dark green, and complex alteration ("altered"). To monitor and account for density changes associated with alteration, we use TiO_2 for normalization since it is relatively fluid-immobile during seafloor alteration [e.g., *Bach et al*., 2001; *Paul et al*., 2006]. To indicate the alteration-induced change we use the ratio of $(C_x/C_{Ti})_A/(C_x/C_{Ti})_F$, where C_x and C_{Ti} indicate the concentrations of element "x" and TiO_2 and subscripts "$_A$" and "$_F$" indicate the C_x/C_{Ti} ratios in altered and fresh samples, respectively.

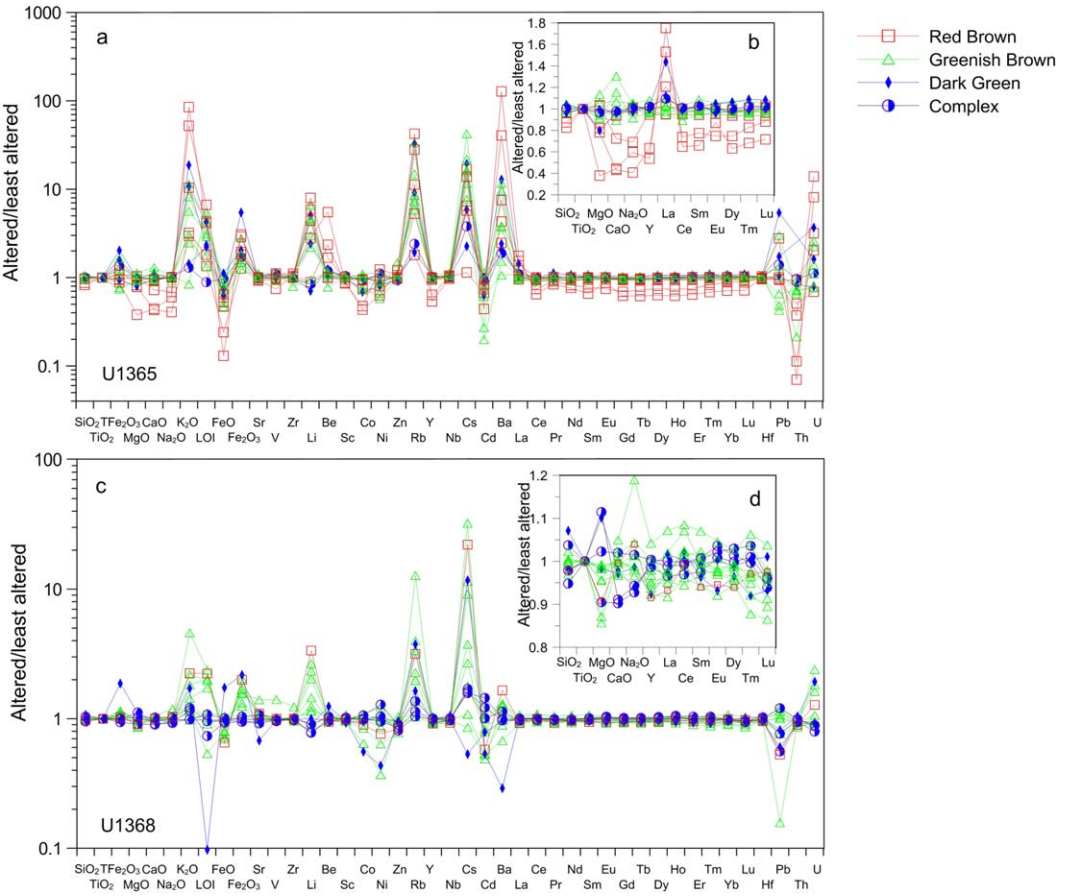

Figure 5. Patterns of elemental ratios of altered/least altered part in the sample pairs normalized to TiO_2.

Ratios of $(C_x/C_{Ti})_A/(C_x/C_{Ti})_F$ for Site U1365 and U1368 sample pairs are shown in supporting information Table S4 and plotted in Figure 5. The most prominent changes for both sites are alteration-induced increases in alkalis (Cs, Rb, K, and Li), Fe_2O_3, Be, LOI, Pb, and Ba and decreases in CaO, MgO, Na_2O, FeO, Co, Ni, and Cd. The changes of total iron (TFe_2O_3) are not obvious relative to the dramatic increases of ferric iron (Fe_2O_3) and decreases of ferrous iron (FeO). These changes are consistent with our petrographic and geochemical observations of oxidative alteration. Increased K and decreased MgO are consistent with elemental changes caused by seafloor alteration at low temperatures, which are related to clay mineral precipitation and alteration of primary mineralogy including plagioclase and olivine. Nb, Zr, and Hf remain immobile, with no significant change observed. A lack of noticeable change in Sr concentration (Figure 5) suggests that Sr exchange during interactions between seawater and basalt may have taken place, countering the suggestion that through alteration ocean crust is a sink for Sr [*Kawahata et al*., 1987; *Krolikowska-Ciaglo et al*., 2005].

Red/brown alteration accounts for 3.5% of recovered cores at Site U1365 and represents the strongest increases in K, Cs, Rb, Li, Be, Ba, U, Fe_2O_3, and LOI, and the strongest decreases in SiO_2, MgO, CaO, Na_2O, FeO, and Y (Figure 5). In addition, La is increased, yet Ce to Lu are decreased in Red/brown alteration halos, implying fractionation of La from other REEs during oxidative alteration. Within red/brown halos Th at Site U1365 is strongly depleted relative to REEs, much stronger than in previous research [e.g., *Bienvenu et al*., 1990; *Ma et al*., 2007]. Based on comparison of the concentrations of seawater K, Rb, and Ca with those observed within brown/red halos at Site U1365, we estimate water-rock ratios of 150, 350, and 2000, respectively. These high water/rock ratios, combined with their proximity to veins, fractures, and lava flow boundaries suggest that Site U1365 red/brown halos formed in zones of high, focused fluid flow. Due to the scarcity of red/brown alteration at Site U1368 (0.2% of recovered core), only one sample pair of red/brown

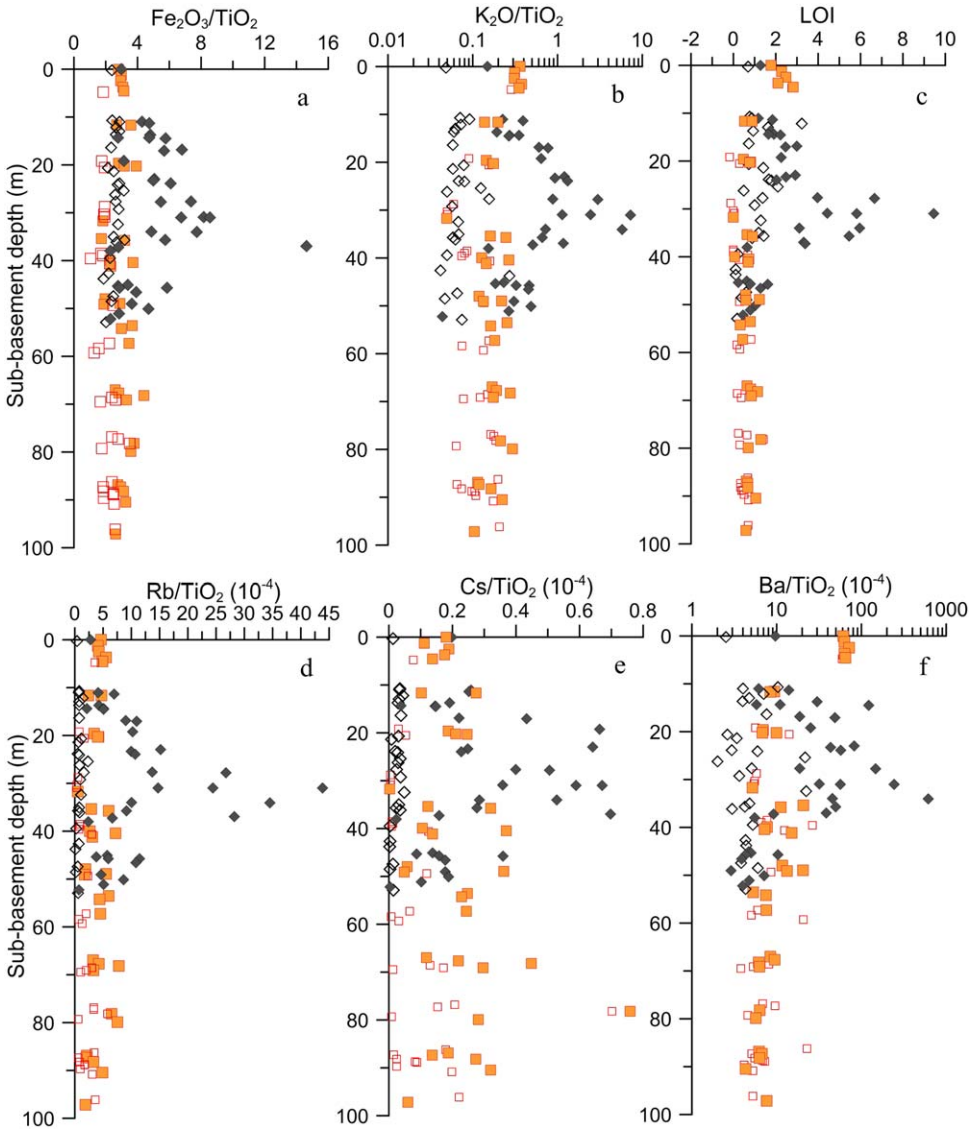

Figure 6. Downhole variations of (a) Fe_2O_3/TiO_2, (b) K_2O/TiO_2, (c) LOI, (d) Rb/TiO_2, (e) Cs/TiO_2, and (f) Ba/TiO_2. Open and filled diamonds indicate fresh (color in gray) and altered (other alteration color) samples for Site U1365; open and filled squares indicate fresh (color in gray) and altered (other alteration color) samples for Site U1368.

alteration was suitable for chemical change calculations. Changes at Site U1368 are broadly similar to those of Site U1365 (Figure 5); however, no significant change of CaO, Be, Y, and REEs was observed.

Greenish brown alteration at both Sites U1365 and U1368 exhibit increases in LOI, K, Li, Rb, Cs, Ba, and U and decreases in Cd and Th. However, unlike red-brown alteration, significant changes of SiO_2, MgO, Na_2O, CaO, Y, Be, and REEs are not observed. Slight increases of LREEs relative to HREEs observed at Site U1368 (Figure 5d) appear unique to greenish brown halos.

Dark green alteration at Sites U1365 and U1368 are similar to those of the greenish brown alteration for most elements (Figure 5) with relatively modest changes compared to the red/brown alteration flanking veins. Complex alteration exhibits the least chemical change compared to other halo types at the both sites, especially for alkalis and LOI, indicating low water/rock ratios.

5.2. Downhole Alteration and Whole Site Elemental Changes

To understand how the alteration-induced elemental changes vary downhole at Sites U1365 and U1368, we have normalized alteration-sensitive elements Fe, Ba, Rb, Ca, K, and LOI to TiO_2 and plotted their variations

downhole (Figure 6). Despite differences in primary evolution (see earlier discussion), the least altered samples exhibit minimal downhole variation in Fe_2O_3/TiO_2, K_2O/TiO_2, LOI, Rb/TiO_2, Cs/TiO_2, and Ba/TiO_2. The most prominent difference between ratios of fresh and altered samples occurs between 20 and 40 msb at Site U1365 (Figure 6), which coincides with a high degree of fracturing/veins (Figure 3) along a lava flow boundary, including the recovery of a basalt breccia and hyaloclastite breccia at ~36 msb. The extent of alteration and chemical change at the 20–40 msb interval imply extensive fluid-rock interaction. At the 20–40 msb interval, the lack of correspondence between core recovery (82–99%), vein/fracture density, or element/TiO_2 peaks suggests that the abundant veins/fractures and strong elemental changes at this interval are not an artifact of variable recovery. We note that despite pockets of very high alteration, many samples at Site U1365 have very low Fe_2O_3/TiO_2, K_2O/TiO_2, LOI, Rb/TiO_2, Cs/TiO_2, and Ba/TiO_2 ratios, supporting petrographic observations that much of Site U1365 basement is relatively fresh and that alteration is concentrated at flow boundaries.

At Site U1368, alteration-induced chemical changes are low compared to Site U1365. K_2O/TiO_2, LOI, and Ba/TiO_2 are most elevated at the uppermost 5 m of basement; however, no other trends were observed for Site U1368 which suggests that alteration, though limited, was pervasive throughout Site U1368 basement.

To quantify the differences in alteration between Sites U1365 and U1368 within whole rocks, we calculate elemental change caused by water-rock interactions using the *Gresens* [1967] method as modified by *Grant* [1986] as follows:

$$C_i^A = M^O/M^A(C_i^O + \Delta C_i) \quad (1)$$

where ΔC_i is the concentration change of element i, C_i^A and C_i^O are concentrations of element i in altered rock (^{A}) and unaltered (^{O}) rock, M^O and M^A are the mass of unaltered and altered rock, respectively. M^O/M^A describe the mass change term, which is determined by calculating the slope of (C^A/C^O) from the immobile element TiO_2. Mass is then factored into C_i^A by multiplying it with M^O/M^A to become $C_{i(Ti)}^A$. Elemental change thus becomes:

$$\Delta C_i = C_{i(Ti)}^A - C_i^O \quad (2)$$

To determine whole site chemical change at Sites U1368 and U1365 (Table 2), averages of chemical change observed in each alteration style were weighted according to their abundance. Sites U1365 and U1368 exhibit prominent gains of TFe_2O_3, K_2O, Fe_2O_3, Li, Rb, Cs, and U, and losses of MgO, CaO, and FeO. One notable difference between the two sites is a gain in Ba at Site U1365 while at Site U1368 Ba is lost. The difference in Ba may reflect differences in calcium carbonate, in which the relatively low abundance of calcium carbonate at Site U1368 may limit Ba uptake. In contrast, the abundance of carbonate at Site U1365 provides a sink for Ba. With the exception of La, we observe a small depletion of REE and Y at Site U1365 (Table 2).

When we compare the total chemical changes of representative elements between Sites U1365 and U1368 (Figure 7), we observe larger increases in TFe_2O_3, Fe_2O_3, CaO, K_2O, Li, Rb, Ba, Pb, and U, and larger losses of FeO at Site U1365 than those at Site U1368. When compared with Site U1368 (13.5 Ma), DSDP 504B (5.9 Ma), DSDP 896 (6 Ma), and ODP 1224 (46 Ma) (Figure 7), Site U1365 exhibits the highest increase in K_2O and highest decrease in CaO, reflecting precipitation of clay minerals and breakdown of primary Ca-bearing mineralogy. Increases of Fe_2O_3 and decreases of FeO at Sites U1365 and U1368 reflect oxidation of FeO, while the elevated total Fe_2O_3 (TFe_2O_3) could have been derived from flowing fluids [e.g., *Mills and Dunk*, 2010; *Bach et al*., 2003].

5.3. Factors Controlling Alteration

The difference in alteration intensity and chemical change between Sites U1365 and U1368 requires consideration of how crustal structure, local heterogeneity, and sediment blanketing and time may be contributing to the overall style and intensity of alteration in seafloor basalts.

5.3.1. Crustal Structure and Local Heterogeneity

Spreading rate is thought to result in fundamental differences in ocean crust structure, lithology, and subsequently, variations in permeability and porosity facilitating hydrothermal alteration [e.g., *Fisher*, 1998; *Alt and Teagle*, 2003; *Alt et al*., 2010]. Sheet lava flows at Site U1365 may act as relatively impermeable

Table 2. Chemical Changes for Cores From Sites U1365 and U1368[a]

	WR-U1365	WR-U1368	WR-1224[b]	Total-1224[b]	WR-1205[c]	Total-504B[d]	Total-896A[d]	Total-417/418[d]
TiO_2 (g/100 g)					0.02			
SiO_2	−0.140	0.003	0.060	0.455	−4.5	0.87	0.69	
Al_2O_3	−0.066	−0.001	0.000	0.018	−0.3	−0.06	−0.10	
TFe_2O_3	0.058	0.105	0.040	0.386	0.6	0.40	0.46	
MnO	−0.001	0.000	0.000	0.000	0			
MgO	−0.067	−0.020	0.020	0.110	−1.5	0.20	0.46	−0.18
CaO	−0.101	−0.011	0.010	0.251	−2	−0.02	−0.03	1.03
Na_2O	−0.015	0.001	0.000	0.021	−0.5	0.02	−0.01	
K_2O	0.113	0.011	0.010	0.016	0.02	0.05	0.09	0.54
P_2O_5	0.000	0.000			−0.1			
LOI	0.245	0.004						
FeO	−0.253	−0.057						
Fe_2O_3	0.339	0.168						
Cr (mg/kg)	−1.253	−1.613						
Sr	−0.069	0.121			−166.6			
V	0.244	0.854						
Zr	−0.195	0.152			−24.7			
Li	2.342	0.346						
Be	0.008	0.001						
Sc	−0.050	−0.056			−0.72			
Co	−0.667	−0.379						
Ni	−1.307	−1.078						
Cu	0.143	−0.133						
Zn	0.360	−0.842						
Ga	−0.079	0.020						
Ge	0.033	0.066						
Rb	1.282	0.366			−2.5			
Y	−0.096	−0.118			−2.5			
Nb	0.008	−0.006			−4.9			
Cd	−0.012	−0.008						
Sn	−0.011	−0.014						
Cs	0.036	0.023			0			
Ba	6.436	−0.115			−51.7			
La	0.021	−0.013			−0.8			
Ce	−0.030	0.010			−1			
Pr	0.000	−0.005			−0.6			
Nd	−0.016	−0.034			−1.7			
Sm	−0.004	−0.002			−0.5			
Eu	−0.002	−0.002			−0.1			
Gd	−0.019	−0.017			−0.5			
Tb	−0.003	−0.003			−0.1			
Dy	−0.015	−0.013			−0.3			
Ho	−0.004	−0.001			−0.1			
Er	−0.010	−0.011			−0.1			
Tm	−0.001	−0.002			−0.02			
Yb	−0.007	−0.010			−0.2			
Lu	−0.001	−0.003			−0.02			
Hf	0.001	−0.005			−0.5			
Pb	0.015	−0.015			−0.3			
Th		−0.002			−0.1			
U	0.007	0.002			0.1			

[a]"WR" indicates calculation induced by whole-rock alteration. "Total" indicates the total changes caused by whole-rock alteration and veins formation.
[b]*Paul et al.* [2006].
[c]*Révillon et al.* [2007].
[d]*Alt et al.* [1996].

boundaries that help focus alteration into zones between each flow. In contrast, recovered ocean crust at Site U1368 comprises ~50% pillow lavas, and thin flows, we would therefore expect grater permeability and more even distribution of alteration. Alteration-induced elemental changes for Site U1365 such as K, Rb, Li, Ba, and U, mirror petrographic results in that the greatest chemical changes are focused between flows, while minimal chemical exchange takes place within flows. The most intensively altered section and the greatest chemical exchange and vein density was observed at 20–40 msb, which might reflect a local heterogeneity in structure controlled fluid flow. The presence of a localized zone of alteration at Site U1365

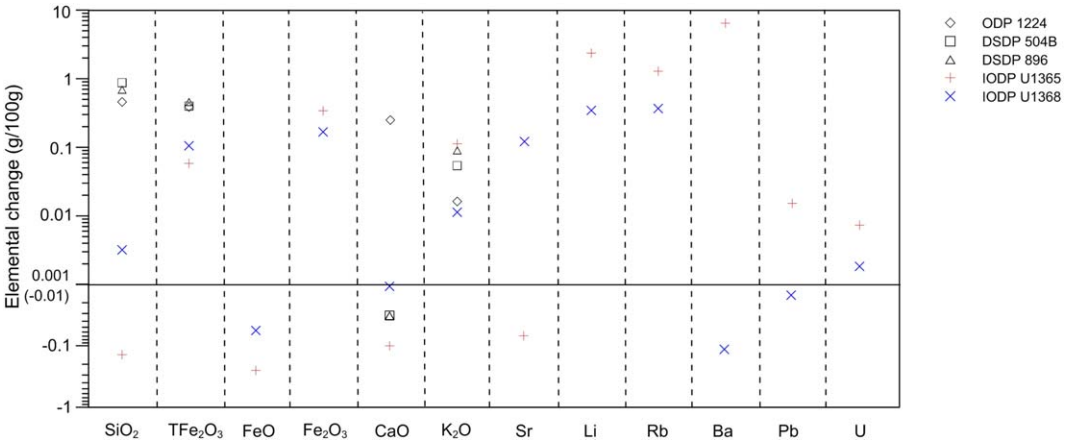

Figure 7. Representative total elemental changes calculated for cores from Sites U1365 and U1368 and comparison with those for other DSDP/ODP sites for the upper most ocean crust.

suggests that focusing of fluid flow along lava flow boundaries depends on local variability in crustal fracturing and channel connectivity.

In contrast, chemical changes at Site U1368 are less pronounced, but more pervasive, which suggests that the permeability of U1368 pillow lavas has facilitated cold seawater circulation throughout upper basement. We also note that where lava flows are recovered at Site U1368, there are correspondingly lower degrees of chemical change and mineral replacement, indicating that lithology still plays a strong control on alteration. We note that the relatively young age of Site U1368, limiting overall exposure time, could have contributed to the observed low alteration. In contrast, at ~100 Ma Site U1365 the formation of new cracks, and reopening of existing cracks over time, as is evident from multiple calcium carbonate vein filling episodes, suggests several episodes of seawater circulation over time, potentially aided by a lack of sediment cover.

5.3.2. Sediment Blanketing and Time

Previous research indicates that sediment blanketing controls communication between the oceans and fluids within the crust [*Lister*, 1972; *Anderson and Hobart*, 1976; *Jacobson*, 1992; *Kurnosov et al*., 2008]. Experiments by *Spinelli et al*. [2004] on typical seafloor sediments demonstrate a fivefold increase in hydraulic impedance when sediment thickness increases from 10 to 100 m. The relationship between hydraulic impedance and sediment thickness suggests that fluid flow into basement is at least in part controlled by sediment thickness, and, therefore controlled by basement topography [*Snelgrove and Forster*, 1996; *Giambalvo et al*., 2000]. Sites U1365 and U1368 are located on a flat ocean floor surrounded by several seamounts [*D'Hondt et al*., 2011]. Thus, both sites may be a location for fluid downwelling, in which their respective sediment thicknesses will exert relatively small hydraulic impedances compared to more thickly sedimented sites. Therefore, both sites are likely to be relatively exposed to seawater. As discussed earlier, evidence for continued oxygenated fluid flow into basement comes from multiple episodes of calcium carbonate precipitation. In addition, optode and electrode measurements at Sites U1365 and U1368 record dissolved oxygen throughout sediment [*D'Hondt et al*., 2011]. The wide spread of red/brown alteration at Site U1365 supports the hypothesis that thin sediment cover facilitated long term seawater-derived oxidative fluid circulation. However, the rare occurrence of saponite and minor sulfides at Site U1365 and U1368 suggest that, despite strong evidence for continued alteration, localized nonoxidative zones are present. These reflect local compositional heterogeneities in fluid evolution. In contrast to Sites U1365 and U1368, drilled basement sites that have endured rapid sedimentary burial and consequently have thick sediment cover (e.g., 332B, 504B, 483, 469, 756D, and 801C) have alteration assemblages consistent with restricted fluid flow and limited oxidative phases [*Kurnosov et al*., 2008].

6. Conclusions

Ocean crust from IODP Sites U1365 (~100 Ma) and U1368 (~13.5 Ma), having endured some of the lowest sedimentation rates on earth, provide a useful means to test the variables that may be controlling alteration

of ocean crust. Alteration of cores from Site U1365, which are composed of sheet lava flows, is focused near flow boundaries and interflow fissures (veins). Alteration at Site U1368, which is composed of a more common arrangement of pillow lavas and sheet flows, is pervasive albeit slight. Secondary mineral phases include celadonite, Fe-oxyhydroxides, saponite, rare quartz, and sulfides, and late stage zeolite and carbonates. These minerals indicate oxidative water/rock interaction at low temperature, accompanied by localized patches where reducing conditions associated with restricted access to oxidative seawater have lead to the formation of saponite, pyrite, and chalcopyrite. Carbonates are wide spread at Site U1365 with multiple episodes of precipitation, but rare at Site U1368 which remains relatively young.

In whole rocks only (no veins/breccia) chemical changes at Site U1365 exhibit larger increases of Fe_2O_3, K_2O, Li, Rb, Ba, Pb, and U, and losses of FeO and CaO than those at Site U1368. The red/brown alteration at Site U1365 has the strongest elemental changes and even caused decreases in Y and REEs (except for La).

Despite the high likelihood of low permeability and low porosity of sheet flows at Site U1365, the calculated total elemental changes, e.g., K, Rb, Li, Ba, and U are significantly higher than those at Site U1368. These results suggest that in addition to crustal structure (focusing of alteration between lava flows), other factors must be contributing to the differences in alteration. The presence of oxygenized seawater at the bottom sediment of Sites U1365 and U1368 suggests that ultralow sedimentation may facilitate continued basement alteration well beyond 10–15 Myr after crustal formation.

Acknowledgments

We thank the Integrated Ocean Drilling Program for providing samples and the shipboard work of the staff and crew during the Expedition 329. This work was financially supported by the Pilot Project of Knowledge Innovation Program, Chinese Academy of Sciences (KZCX2-EW-QN205), the Open Foundation in IOCAS (MGE2011KG05), and the National Natural Science Foundation of China (41376065 and 41176043).

References

Alt, J. C., and J. Honnorez (1984), Alteration of the upper oceanic crust, DSDP Site 417: Mineralogy and chemistry, *Contrib. Mineral. Petrol.*, *87*, 149–169.

Alt, J. C., and D. A. H. Teagle (2003), Hydrothermal alteration of upper oceanic crust formed at a fast-spreading ridge: Mineral, chemical, and isotopic evidence from ODP Site 801, *Chem. Geol.*, *201*, 191–211.

Alt, J. C., C. France-Lanord, P. A. Floyd, P. Castillo, and A. Galy (1992), Low-temperature hydrothermal alteration of Jurassic ocean crust, Site 801, *Proc. Ocean Drill. Program Sci. Results*, *129*, 415–427.

Alt, J. C., D. A. H. Teagle, C. Laverne, D. A. Vanko, W. Bach, J. Honnorez, K. Becker, M. Ayadi, and P. Pezard (1996), Ridge-flank alteration of upper oceanic crust in the Eastern Pacific: Synthesis of results for volcanic rocks of Holes 504B and 896A, *Proc. Ocean Drill. Program Sci. Results*, *148*, 417–434.

Alt, J. C., C. Laverne, R. M. Coggon, D. A. H. Teagle, N. R. Banerjee, S. Morgan, C. E. Smith-Duque, M. Harris, and L. Galli (2010), Subsurface structure of a submarine hydrothermal system in ocean crust formed at the East Pacific Rise, ODP/IODP Site 1256, *Geochem. Geophys. Geosyst.*, *11*, Q10010, doi:10.1029/2010GC003144.

Anderson, R. N., and M. A. Hobart (1976), The relation between heat flow, sediment thickness, and age in the eastern Pacific, *J. Geophys. Res.*, *81*(17), 2968–2989.

Argus, D. F., and R. G. Gordon (1991), No-net-rotation model of current plate velocities incorporating plate motion model NUVEL-1, *Geophys. Res. Lett.*, *18*(11), 2039–2042.

Bach, W., J. C. Alt, Y. Niu, S. E. Humphris, J. Erzinger, and H. J. B. Dick (2001), The geochemical consequences of late stage low-grade alteration of lower ocean crust at the SW Indian Ridge: Results from ODP Hole 735 (Leg 176), *Geochim. Cosmochim. Acta*, *65*, 3267–3287.

Bach, W., B. Peucker-Ehrenbrink, S. R. Hart, and J. S. Blusztajn (2003), Geochemistry of hydrothermally altered oceanic crust: DSDP/ODP Hole 504B—Implications for seawater-crust exchange budgets and Sr- and Pb-isotopic evolution of the mantle, *Geochem. Geophys. Geosyst.*, *4*(3), 8904, doi:10.1029/2002GC000419.

Bienvenu, P., H. Bougault, J. L. Joron, M. Treuil, and L. Dmitriev (1990), MORB alteration: Rare-earth element/non-rare-earth hygromagmaphile element fractionation, *Chem. Geol.*, *82*, 1–14.

Böhlke, J. K., J. Honnorez, and B.-M. Honnorez-Guerstein (1980), Alteration of basalts from Site 396B, DSDP: Petrographic and mineralogic studies, *Contrib. Mineral. Petrol.*, *73*, 341–364.

Burns, S. J., P. A. Baker, and H. Elderfield (1992), Timing of carbonate mineral precipitation and fluid flow in sea-floor basalts, northwest Indian Ocean, *Geology*, *20*, 255–258.

D'Hondt, S., et al. (2009), Subseafloor sedimentary life in the South Pacific Gyre, *Proc. Natl. Acad. Sci. U.S.A.*, *106*, 11,651–11,656, doi:10.1073/pnas.0811793106.

D'Hondt, S., F. Inagaki, C. A. Alvarez Zarikian, and the Expedition 329 Scientists (2011), *Proceedings of Integrated Ocean Drilling Program*, vol. 329, Integrated Ocean Drill. Program Manage. Int. Inc., Tokyo, doi:10.2204/iodp.proc.329.103.2011.

Divins, D. L. (2003), Total Sediment Thickness of the World's Oceans & Marginal Seas, NOAA Natl. Geophys. Data Cent., Boulder, Colo. [Available at http://www.ngdc.noaa.gov/mgg/sedthick/sedthick.html.]

Fisher, A. T. (1998), Permeability within basaltic oceanic crust, *Rev. Geophys.*, *36*(2), 143–182.

Fisher, A. T., et al. (2003a), Hydrothermal recharge and discharge across 50 km guided by seamounts on a young ridge flank, *Nature*, *421*, 618–621, doi:10.1038/nature01352.

Fisher, A. T., C. A. Stein, R. N. Harris, K. Wang, E. A. Silver, M. Pfender, M. Hutnak, A. Cherkaoui, R. Bodzin, and H. Villinger (2003b), Abrupt thermal transition reveals hydrothermal boundary and role of seamounts within the Cocos Plate, *Geophys. Res. Lett.*, *30*(11), 1550, doi:10.1029/2002GL016766.

Giambalvo, E. R., A. T. Fisher, J. T. Martin, L. Darty, and R. Lowell (2000), Origin of elevated sediment permeability in a hydrothermal seepage zone, eastern flank of the Juan de Fuca Ridge, and implications for transport of fluid and heat, *J. Geophys. Res.*, *105*(B1), 913–928.

Gillis, K. M., and P. T. Robinson (1988), Distribution of alteration zones in the upper oceanic crust, *Geology*, *16*, 262–266.

Grant, J. A. (1986), The isocon diagram—A simple solution to Gresens' equation for metasomatic alteration, *Econ. Geol.*, *81*, 1976–1982.

Gresens, R. L. (1967), Composition-volume relationships of metasomatism, *Chem. Geol.*, *2*, 47–55.

Grevemeyer, I., N. Kaul, H. Villinger, and W. Weigel (1999), Hydrothermal activity and the evolution of the seismic properties of the upper oceanic crust, *J. Geophys. Res.*, *104*(B3), 5069–5079.

Hart, R. A. (1970), Chemical exchange between sea water and deep ocean basalts, *Earth Planet. Sci. Lett.*, *9*, 269–279.
Hart, S. R., and H. Staudigel (1982), The control of alkalies and uranium in seawater by ocean crust alteration, *Earth Planet. Sci. Lett.*, *58*, 202–212.
Hart, S. R., and H. Staudigel (1986), Ocean crust vein mineral deposition: Rb/Sr ages, U-Th-Pb geochemistry, and duration of circulation at DSDP sites 261, 462 and 516, *Geochim. Cosmochim. Acta*, *50*(12), 2751–2761.
Hasterok, D., D. S. Chapman, and E. E. Davis (2011), Oceanic heat flow: Implications for global heat loss, *Earth Planet. Sci. Lett.*, *311*, 386–395.
Hauff, F., K. Hoernle, and A. Schmidt (2003), Sr-Nd-Pb composition of Mesozoic Pacific oceanic crust (Site 1149 and 801, ODP Leg 185): Implications for alteration of ocean crust and the input into the Izu-Bonin-Mariana subduction system, *Geochem. Geophys. Geosyst.*, *4*(8), 8913, doi:10.1029/2002GC000421.
Hutnak, M., A. T. Fisher, R. N. Harris, C. Stein, K. Wang, G. Spinelli, M. Schindler, H. Villinger, and E. Silver (2008), Large heat and fluid fluxes driven through mid-plate outcrops on ocean crust, *Nat. Geosci.*, *1*, 611–614, doi:10.1038/ngeo264.
Jacobson, R. S. (1992), Impact of crustal evolution on changes of the seismic properties of the uppermost ocean crust, *Rev. Geophys.*, *30*(1), 23–42.
Jarrard, R. D., L. J. Abrams, R. Pockalny, R. L. Larson, and T. Hirono (2003), Physical properties of upper oceanic crust: Ocean Drilling Program Hole 801C and the waning of hydrothermal circulation, *J. Geophys. Res.*, *108*(B4), 2188, doi:10.1029/2001JB001727.
Johnson, H. P., and M. J. Pruis (2003), Fluxes of fluid and heat from the oceanic crustal reservoir, *Earth Planet. Sci. Lett.*, *216*, 565–574.
Kawahata, H., M. Kusakabe, and Y. Kikuchi (1987), Strontium, oxygen, and hydrogen isotope geochemistry of hydrothermally altered and weathered rocks in DSDP Hole 504B, Costa Rica Rift, *Earth Planet. Sci. Lett.*, *85*, 343–355.
Krolikowska-Ciaglo, S., F. Hauff, and K. Hoernle (2005), Sr-Nd isotope systematics in 14–28 Ma low-temperature altered mid-ocean ridge basalt from the Australian Antarctic Discordance, Ocean Drilling Program Leg 187, *Geochem. Geophys. Geosyst.*, *6*, Q01001, doi:10.1029/2004GC000802.
Kurnosov, V. B., B. P. Zolotarev, A. V. Artamonov, S. M. Lyapunov, G. L. Kashinzev, O. V. Chudaev, A. L. Sokolova, and S. A. Garanina (2008), Technical note: Alteration effects in the upper oceanic crust—Data and comments, in *Transactions of the Geological Institute*, vol. 581, Geol. Inst., Moscow.
Laverne, C., A. Belarouchi, and J. Honnorez (1996), Alteration mineralogy and chemistry of the upper oceanic crust from Hole 896a, Costa Rica Rift, *Proc. Ocean Drill. Program Sci. Results*, *148*, 151–170.
Lister, C. R. B. (1972), On the thermal balance of a mid-ocean ridge, *Geophys. J. R. Astron. Soc.*, *26*, 515–535.
Ma, J. L., G. J. Wei, Y. G. Xu, W. G. Long, and W. D. Sun (2007), Mobilization and re-distribution of major and trace elements during extreme weathering of basalt in Hainan Island, South China, *Geochim. Cosmochim. Acta*, *71*, 3223–3237.
Mills, R. A., and R. M. Dunk (2010), Tracing low-temperature fluid flow on ridge flanks with sedimentary uranium distribution, *Geochem. Geophys. Geosyst.*, *11*, Q08009, doi:10.1029/2010GC003157.
Nedimović, M. R., S. M. Carbotte, J. B. Diebold, A. J. Harding, J. P. Canales, and G. M. Kent (2008), Upper crustal evolution across the Juan de Fuca ridge flanks, *Geochem. Geophys. Geosyst.*, *9*, Q09006, doi:10.1029/2008GC002085.
Paul, H. J., K. M. Gillis, R. M. Coggon, and D. A. H. Teagle (2006), ODP Site 1224: A missing link in the investigation of seafloor weathering, *Geochem. Geophys. Geosyst.*, *7*, Q02003, doi:10.1029/2005GC001089.
Pichler, T., W. I. Ridley, and E. Nelson (1999), Low-temperature alteration of dredged volcanics from the Southern Chile Ridge: Additional information about early stages of seafloor weathering, *Mar. Geol.*, *159*, 155–177.
Révillon, S., D. A. H. Teagle, P. Boulvais, J. Shafer, and C. R. Neal (2007), Geochemical fluxes related to alteration of a subaerially exposed seamount: Nintoku seamount, ODP Leg 197, Site 1205, *Geochem. Geophys. Geosyst.*, *8*, Q02014, doi:10.1029/2006GC001400.
Richardson, S. H., S. R. Hart, and H. Staudigel (1980), Vein mineral ages of old oceanic crust, *J. Geophys. Res.*, *85*(B12), 7195–7200.
Rohr, K. M. M. (1994), Increase of seismic velocities in upper oceanic crust and hydrothermal circulation in the Juan de Fuca plate, *Geophys. Res. Lett.*, *21*(19), 2163–2166.
Schramm, B., T. C. W. Devey, K. M. Gillis, and K. Lackschewitz (2005), Quantitative assessment of chemical and mineralogical changes due to progressive low-temperature alteration of East Pacific Rise basalts from 0 to 9 Ma, *Chem. Geol.*, *218*, 281–313.
Snelgrove, S. H., and C. B. Forster (1996), Impact of seafloor sediment permeability and thickness on off-axis hydrothermal circulation: Juan de Fuca Ridge eastern flank, *J. Geophys. Res.*, *101*(B2), 2915–2925.
Spinelli, G. A., E. R. Giambalvo, and A. T. Fisher (2004), Sediment permeability, distribution, and influence on fluxes in oceanic basement, in *Hydrogeology of the Oceanic Lithosphere*, edited by E. E. Davis and H. Elderfield, Cambridge Univ. Press, Cambridge, U. K.
Staudigel, H., and S. R. Hart (1983), Alteration of basaltic glass: Mechanisms and significance for the oceanic crust-seawater budget, *Geochim. Cosmochim. Acta*, *47*, 37–350.
Staudigel, H., K. Muehlenbachs, S. H. Richardson, and S. R. Hart (1981a), Agents of low temperature ocean crust alteration, *Contrib. Mineral. Petrol.*, *77*(2), 150–157.
Staudigel, H., S. R. Hart, and S. H. Richardson (1981b), Alteration of the oceanic crust: Processes and timing, *Earth Planet. Sci. Lett.*, *52*(2), 311–327.
Staudigel, H., K. Gillis, and R. Duncan (1986), K/Ar and Rb/Sr ages of celadonites from the Troodos ophiolite, Cyprus, *Geology*, *14*, 72–75.
Stein, C. A., and S. Stein (1994), Constraints on hydrothermal heat flux through the oceanic lithosphere from global heat flow, *J. Geophys. Res.*, *99*(B2), 3081–3095.
Sun, S. S., and W. F. McDonough (1989), Chemical and isotopic systematics of oceanic basalts: Implications for mantle composition and processes, *Geol. Soc. Spec. Publ.*, *42*, 313–345.
Talbi, E. H., and J. Honnorez (2003), Low-temperature alteration of mesozoic oceanic crust, Ocean Drilling Program Leg 185, *Geochem. Geophys. Geosyst.*, *4*(5), 8906, doi:10.1029/2002GC000405.
Thompson, G. (1983), Hydrothermal fluxes in the Ocean, *Chem. Oceanogr.*, *8*, 271–337.
Wheat, C. G., and M. J. Mottl (2000), Composition of pore and spring waters from Baby Bare: Global implications of geochemical fluxes from a ridge flank hydrothermal system, *Geochim. Cosmochim. Acta*, *64*, 629–642.
Zhang, G. L., C. Smith_Duque, H. Li, C. Zarikian, S. D'Hondt, and F. Inagaki (2012), Geochemistry of basalts from IODP site U1365: Implications for magmatism and mantle source signatures of mid-Cretaceous Osbourn Trough, *Lithos*, *144–145*, 73–87.
Zhang, G. L., L. H. Chen, and S. Z. Li (2013), Mantle dynamics and generation of a geochemical mantle boundary along the East Pacific Rise-Pacific/Antarctic ridge, *Earth Planet. Sci. Lett.*, *383*, 153–163.